RSC Advances

PAPER

Cite this: *RSC Adv.*, 2016, **6**, 41074

Ammonolysis of polycrystalline and amorphized gallium arsenide GaAs to polytype-specific nanopowders of gallium nitride GaN†‡

Mariusz Drygaś,[a] Piotr Jeleń,[b] Marta Radecka[b] and Jerzy F. Janik*[a]

Received 3rd March 2016
Accepted 16th April 2016

DOI: 10.1039/c6ra05706c

www.rsc.org/advances

Convenient single-step N-for-As metathesis reactions of gallium arsenide GaAs with ammonia NH_3 at temperatures in the range 650–950 °C for 6–90 hours afforded in this oxygen-free system high yields of pure nanocrystalline powders of the wide bandgap semiconductor gallium nitride GaN. High energy ball milling *via* noticeable amorphization of the monocrystalline cubic GaAs substrate enabled complete ammonolysis and nitride preparation at lower temperatures and shorter times relative to manual grinding. Under the applied conditions, all by-products were removed as volatiles affording pure GaN nanopowders. Reaction-controlled average crystallite sizes ranged from a few to a few tens of nanometers. When compared to the related ammonolysis reactions of cubic GaP and cubic GaSb which yielded, respectively, either the hexagonal polytype only or mixtures of mostly hexagonal with some cubic GaN polytypes, here, the nitride could be made both as solely hexagonal and as a mixture of two polytypes in a wide composition range. All this supports diverse reaction pathways which were found to be closely correlated with substrate grain size characteristics. The ball milled fine GaAs particles afforded only hexagonal or hexagonal GaN-enriched mixtures pointing to predominantly thermodynamic reaction control. Under similar conditions, the manually ground coarser GaAs particles yielded cubic GaN-enriched mixtures, instead, consistent with prevailing topochemical control.

Introduction

Gallium nitride GaN is a prime example of a wide bandgap semiconductor (3.4 eV for hexagonal polytype and 3.2 eV for cubic polytype) that offers a multitude of advantages compared to the classic silicon (1.1 eV) or gallium arsenide GaAs-based (1.4–1.5 eV) semiconductors, especially, for demanding applications in modern optoelectronics.[1,2] The reported synthesis methods of GaN are mostly concerned with GaN-based nanostructured film formation or with making monocrystalline optoelectronic device supports for blue light emitters. At the same time, the progress in developing simple and high-yield synthesis methods for GaN nanopowders is not yet satisfactory as exemplified by some of the reviews on the subject.[3] We touched this issue first-hand when we needed significant quantities of GaN nanopowders for our otherwise successful studies of the nitride's nanopowder sintering.[4] Despite having at hand quite a few of our own preparations,[5] still, we would have appreciated a simple, high-yield, polytype and size-controlled while economically efficient synthesis of the nanopowder.

At this point, it is worth noting that there is a relatively small difference in standard total energies between the thermodynamically stable hexagonal polytype and the unstable cubic polytype of GaN. The total energy of cubic GaN (c-GaN) is higher merely by 9.88 meV per atom or 16 meV per unit than that of the stable hexagonal GaN (h-GaN).[6] These data suggest that the formation of the nitride's metastable cubic phase can be quite realistic in practice given a suitable choice of experimental conditions. In this regard, there are known reports confirming the preparation of pure c-GaN, mostly, as thin films[7] or polycrystalline products from autoclave syntheses,[8] whereas under moderate conditions the c-GaN is often accompanied by the h-GaN in physical mixtures of the polytypes but, also, *via* stacking faults in multidomain nanostructures.[9] Concluding this aspect, for suitable reaction systems a fine interplay and competition of the thermodynamic and kinetic/topochemical factors will decide about the GaN polytype make-up in the nitridation product.

Along these lines, we have recently reported on metathetical ammonolysis of some of the gallium pnictides such as cubic gallium phosphide c-GaP[10] and cubic gallium antimonide c-GaSb,[11] which yielded various GaN nanopowders in one

[a]*AGH University of Science and Technology, Faculty of Energy and Fuels, al. Mickiewicza 30, 30-059 Krakow, Poland. E-mail: janikj@agh.edu.pl*

[b]*AGH University of Science and Technology, Faculty of Materials Science and Ceramics, al. Mickiewicza 30, 30-059 Krakow, Poland*

† Dedicated to Prof. Emer. Aleksander Karcz, AGH University of Science and Technology, Krakow, Poland on the occasion of his 77th birthday.

‡ Electronic supplementary information (ESI) available. See DOI: 10.1039/c6ra05706c

step and high yields. It is worth mentioning that large-scale preparations of bulk crystals of these substrates, being themselves the valuable semiconductors, are well developed (Czochralski method) and, additionally, significant amounts of the materials appear to be available as post-processing wastes in the electronic industry. Regarding the c-GaP/NH_3 system, all reactions at 900–1150 °C for 6–60 h afforded exclusively the stable hexagonal h-GaN polytype with reaction-controlled average crystallite sizes of up to a few tens of nanometers. The application of high energy ball milled GaP substrate resulted in a specific reaction pathway with h-GaN nanowire formation whereas manual grinding yielded irregularly shaped h-GaN nanoparticles. In the c-GaSb/NH_3 system, the reactions at 900–1000 °C for 36–170 h gave mixtures of the major hexagonal h-GaN polytype and the minor metastable cubic c-GaN polytype regardless of the way the substrate was ground. Interestingly, the application of ball milling resulted in the comparable quantities of h-GaN in the 66–68% range, suppressing greatly the temperature/time conditions. In both systems, the formation of the stable h-GaN was a manifestation of the thermodynamics playing the major role in reaction mechanism *via*, likely, initial decomposition of the pnictide towards transient Ga droplets followed by reactions with ammonia or *via* gas phase ammonolysis reactions of the volatilized pnictide. The formation of the metastable c-GaN could be linked to topochemically controlled N-for-Sb replacement in the cubic GaSb taking place with lattice type preservation.

We also contributed to studying the known reactions of cubic gallium arsenide c-GaAs with ammonia[12] which in our hands yielded increased up to 90% proportions of the cubic c-GaN.[13] In that study, we compared the ammonolysis of bulk platelets and manually ground c-GaAs. However, no clear-cut conclusion regarding the impact of these two substrate forms on GaN polytype formation could be reached, which we now ascribe to relatively insignificant differences in the then available reaction surfaces. Considering the results for the related c-GaSb/NH_3 system,[11] herein, we essentially altered the grain size/surface characteristics by employing high energy ball milling of the monocrystalline c-GaAs substrate. Not only this, but an unexpected side-decomposition of GaAs and its partial amorphization upon milling crucially effected outcome of the thermodynamic *vs.* topochemical factor competition in the subsequent nitridation reactions. In this regard, it is worth reiterating that molten elemental gallium (m.p. 29 °C) from GaAs decomposition is going to favor the formation of the thermodynamically stable h-GaN. In contrast, yet unspecified conditions supporting kinetically controlled topochemical N-for-As replacement in c-GaAs will yield the metastable c-GaN if winning the competition with arsenide decomposition rate. Given the lack of precise theoretical predictions, the question whether it is possible or not to pinpoint the right conditions for an exclusive formation of either polytype in the system remains a domain for experimental verification.

Experimental

Synthesis

Monocrystalline wafer chunks of commercial quality gallium arsenide GaAs with orientation [100] were acquired generously as waste material from the Institute of Electronic Materials Technology, Warszawa, Poland. Material grinding was done by two methods. In manual grinding, a few chunks of monocrystal were placed in an agate mortar and ground for approximately 10 minutes to afford a black powder. For deep grinding by wet high energy ball milling, a few grams of chunks crashed to sizes below *ca.* 1 mm were placed in a grinding bowl of the FRITSCH Pulverisette 7 planetary ball mill onto which 10 ml of dry xylene were added. Wet milling conditions are applied to minimize attrition of the grinding balls made of tungsten carbide WC. Either one (short milling) or twenty (long milling) 3 minute intermittent grinding periods were applied at 900 rpm, each separated by a 10 minute break to prevent overheating of the bowl's content. After each grinding period, the bowl warmed up to 50–60 °C much below the boiling point of xylene, 140 °C. Following recovery from the bowl, the paste was evacuated for 1 hour to remove volatiles affording a precursor powder. A batch of *ca.* 1 g of the powder or, in two cases, a 10 × 10 mm piece of an original GaAs wafer, was placed in an open-ended alumina boat and inserted into a ceramic reactor in a tube furnace. Prior to heating, the system was purged with high purity NH_3, 99.999%, 30 min, 0.05 L min^{-1}, and such a flow rate was maintained throughout the reaction. The reaction temperatures, 650–900 °C for powders and 900–950 °C for bulk wafers, were attained with a heating rate of 5 °C min^{-1}. Hold times, 6–90 h, were suitably adjusted at each temperature level to afford complete nitridation. The reactions were carried out for both the manually ground and ball milled GaAs powders. Upon cooling products to room temperature under flowing ammonia, each sample was evacuated for 30 minutes to remove volatiles. The final products were gray brownish, loosely agglomerated powders.

Characterization

Particle size distribution for substrate powders was measured by dynamic light scattering on Nanosizer-ZS of Malvern Instruments. Standard 5-point BET specific surface areas, mesopore surface areas, and average mesopore diameter (the latter two based on BJH theory applied to the desorption part of the isotherm hysteresis) were determined by low temperature nitrogen adsorption on Micromeritics Gemini 2380. Selected products were investigated by photoelectron spectroscopy XPS (Vacuum Systems Workshop Ltd., Mg anode with photon energy of 1253.6 eV). All substrates and products were characterized by standard powder XRD analysis (Empyrean PANalytical, Cu Kα source; $2\Theta = 10–110°$). Average crystallite sizes were evaluated from Scherrer's equation applying the Rietveld refinement method. Solid-state ^{71}Ga MAS NMR spectra were acquired on the APOLLO console (Tecmag) at the magnetic field of 7.05 T produced by a 89 mm bore superconducting magnet (Magnex). A Bruker HP-WB high-speed MAS probe equipped with a 4 mm

zirconia rotor and KEL-F cap was used to record the MAS NMR spectra at the spinning rates of 8 kHz. The resonance frequency was equal to 91.385 MHz and a single 2 μs rf pulse was used, which corresponded to $\pi/4$ flip angle in the liquid. The acquisition delay used in accumulation was 1 second and the typical number of acquisitions ranged from 1000 to 4000. The frequency scale in ppm was referenced to $Ga(NO_3)_3$ (1 M in D_2O). All resonance positions were uncorrected for the second-order quadrupolar shift. Micro-Raman analysis was done by HORIBA LabRAM HR spectrometer with 532 nm laser, sample power of 20 mW, accumulation time 10 s and 2 scans, confocal hole 1000 μm with long-focus length. UV-vis data were collected on a Perkin-Elmer spectrophotometer Lambda 35 equipped with a 50 mm integrating sphere. SEM/EDX data were acquired with a Hitachi Model S-4700 scanning electron microscope.

Results and discussion

The chemistry behind the ammonolytical nitridation of GaAs can be summarized by a thermodynamically supported simplified reaction of the type $GaAs + NH_3 \rightarrow GaN + AsH_3(As + 3/2H_2)$ paralleling the related systems of GaP/NH_3 [10] and $GaSb/NH_3$.[11] The arsine AsH_3 by-product is a gas stable at ambient conditions (ΔH_f^{298} $AsH_3 = -66.4$ kJ mol^{-1}) and known to decompose into several species including As, As_2, and As_4 vapors at increased temperatures, especially, higher than 230 °C.[14] Under the experimental conditions of complete nitridation, we noted condensation of by-product vapors into shining mirrors of elemental arsenic on colder parts of the set-up leaving a pure GaN product in the hot zone with no separation efforts. No elemental arsenic was detected either by XRD or XPS in the completely nitrided products.

It needs to be pointed out that GaAs shows a limited thermal stability in the applied temperature range of 650–950 °C. The congruent evaporation of GaAs under vacuum takes place at 625–690 °C and at these and higher temperatures the vapors are enriched in arsenic leaving molten droplets of elemental gallium on GaAs surfaces.[15] Actually, such Ga droplet formation and stability have received increased attention in the development of relevant droplet epitaxy techniques.[15a,16] Progress of GaAs decomposition under the flow of ammonia may be somewhat retarded as may be volatile arsenic removal. The relatively low decomposition temperatures of GaAs may thus create conditions for ammonia reacting with the resulting gallium droplets towards the thermodynamically favored hexagonal polytype of GaN before reaching a threshold for efficient topochemical nitridation and cubic polytype formation.

When considering the target ammonolytical nitridation of GaAs, it is worth to overview the compound's reactivity towards nitrogen sources and formation of the stable or metastable intermediate GaAsN, formally, $GaAs_{1-x}N_x$ alloy. This issue has been well reviewed and supported by computational studies.[17] The cubic end-members of the alloy, c-GaAs and c-GaN, show the lattice constants *a* equal to 5.65 Å and 4.50–4.51 Å, respectively. The *ca.* 20% difference in the constants is significant enough to warrant the existence of a large miscibility gap in this alloy. However, the formation of diluted substitutional gallium arsenide nitride has been found plausible both theoretically and experimentally. For the As-rich side of compositions (formally, N-for-As substitutions in GaAs), many theoretical and experimental studies have supported N-concentrations in GaAsN of up to a few percent in bulk materials whereas levels in the 20–30% range have been reported for specifically grown thin films. For the less studied N-rich side of compositions (As-for-N substitution in GaN), alloys with up to 6–7% As-contents were claimed, which characteristically showed the blue luminescence.[18] In the recent report on MBE growth of diluted GaAsN alloys by surface nitridation of GaAs with nitrogen plasma, the N-contents in the 1–5% range were produced.[19] From the collected data on such systems, a gradual and topochemically controlled replacement of As with N in the c-GaAs crystallites is plausible and can, eventually, lead to the cubic polytype of GaN. The relative closeness of the lattice constants and mixed alloy formation/stability may not, however, be the decisive factors in the nitridation towards a specific GaN polytype. In this regard, the presumed conversion of c-GaP to c-GaN with the respective lattice constants *a* of 5.45 and 4.50 Å was shown to produce exclusively the hexagonal polytype of GaN under a wide range of experimental conditions, instead, since the determinant properties of the system solely favored the reaction control by thermodynamics over topochemistry.[10]

Fig. 1 shows three particle size distribution curves, *i.e.*, one for manually ground (GaAs-MG) and two for high energy ball milled GaAs, the latter including a short (GaAs-SBM) and long (GaAs-LBM) wet milling. The size distribution curves are characteristic of two prevailing size modes that are centered at *ca.* 10–20 μm and *ca.* 2–3 μm. The former particle size mode is predominant in GaAs-MG whereas the latter one dominates in GaAs-LBM, which is consistent with a deeper/more efficient grinding by ball milling. Interestingly, in both wet ball milled samples there is an evolving fraction of extremely small particles with sizes of several tens of nanometer, which is especially clearly seen after long milling (see, the tail below 0.1–0.2 μm/100–200 nm). This particle size mode points out to a susceptibility of GaAs to efficient deep grinding and producing a share of extremely small particles in the nanosized range. In terms of the relevant XRD pattern characteristics, this manifests itself in peak broadening and is often described as a material amorphization (*vide infra*). It is also associated with visibly increased particle surface areas of enhanced reactivity compared to manual grinding.

The typical SEM morphologies of the GaAs substrates and the resulting nitride nanopowders are shown in Fig. 2. In the top row, it is clearly seen that the manually ground GaAs (top row, left) consists of the relatively large solid-body particles compared with the long wet ball milled GaAs (top row, middle and right). In the latter case, the large particles appear to be secondary agglomerates made of much smaller and size-diverse solid fragments. Certainly, the presence of such agglomerates if bound tightly enough impacts the interpretation of the particle size distribution curves. It both explains the detection of the large particles and, at the same time, supports a likely higher share of the smallest particles in the nanosized range, which are

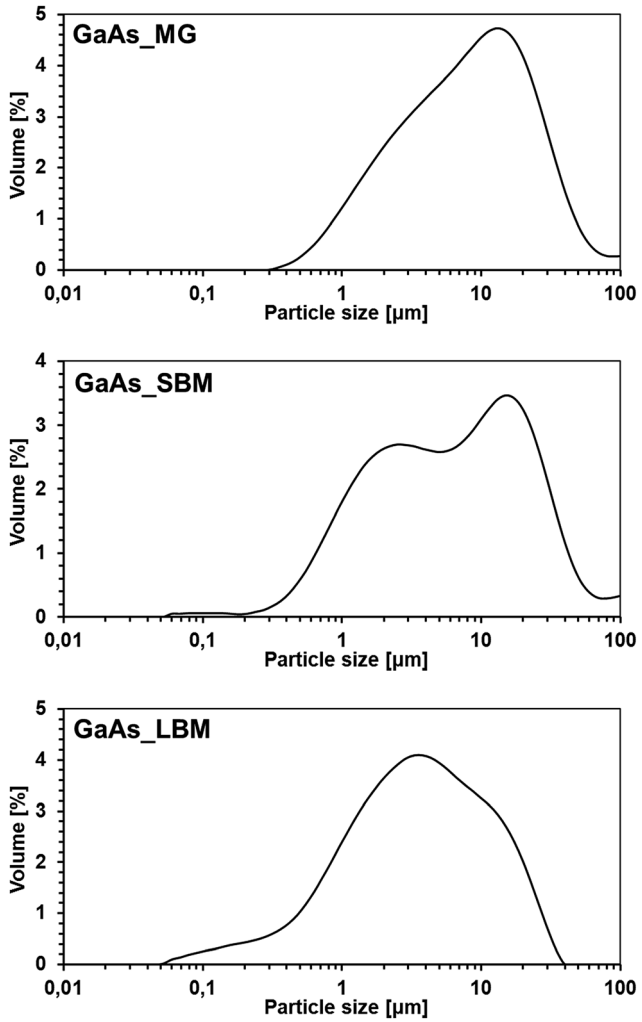

Fig. 1 Particle size distribution curves of ground GaAs: top – manually ground, middle – short wet ball milled, bottom – long wet ball milled.

extremely prone to agglomeration, than indicated straight in the curves (Fig. 1). The nitride products from the two grinding methods and both conversion temperatures exhibit overall the surprisingly uniform particle shapes and habit as well as extensive agglomeration. In the case of the 700 °C-derived nanopowder from the manually ground precursor, the aggregation habit seems to be reminiscent of the initial "waving" texture of a precursor particle (middle row, left).

The case of the GaAs wafer nitridation, 900 °C, 6 h, which was done for comparative purposes, is illustrated in Fig. 3. A distinct and relatively thin (*ca.* 2.5 μm) compact surface layer is seen in addition to the interior made of agglomerated large spherical features (*ca.* 10–30 μm) of GaN (*vide infra*, XRD results). These spheres appear to be forming at least a few quite uniform in thickness layers stacked one upon the other in the sample interior. The spheres are themselves made of tightly agglomerated smaller crystallites of well evolved facets in the microcrystalline range. Some of the crystallites appear to be interfused forming tight clusters. All this is consistent with a different nitridation mechanism and crystallite growth on the wafer surface compared with its interior. As a result, the surface layer seems to be made of perpendicular well aligned microcrystallites resulting from diffusion controlled reactions that start on a flat wafer surface. It is tempting to assign it to mostly thermodynamic nitridation producing h-GaN. The spherical aggregates of interior are then formed from liquid droplets and multi-seed crystallization upon nitridation. The most likely candidate for forming the liquid phase is elemental Ga so that the conversion in this case could first involve an extensive decomposition of GaAs in the undersurface layers followed by reactions of Ga with NH_3 along $Ga + NH_3 \rightarrow GaN + 3/2H_2$. In such the Ga-liquid assisted synthesis the formation of the thermodynamically stable h-GaN would be favored.

Table 1 contains results of the low temperature nitrogen adsorption study of the GaAs substrates and the GaN nanopowder products aimed at determination of standard surface area parameters. The common BET specific surface areas of the order of a few to a few tens of $m^2\ g^{-1}$ are typical for macroporous to low mesoporous materials. This is supported by the comparable values of the calculated BJH mesopore specific surface areas. Starting with the macroporous powders of the GaAs substrates, GaN nanopowders with *ca.* 2–3 times greater BET surface areas are obtained. First, it is apparent that employing the ball milling, especially, long milling results in GaAs with significantly increased particle surface areas at the start. And second, this later translates to the corresponding 2–3-fold higher surface area of the GaN products. In effect, the nitridation conversion is associated with significant surface area increases for products and with some size/porosity constraints as previously reported.[5j]

The XRD patterns for the manually ground and long ball milled GaAs as well as for the bulk GaAs wafer are shown in Fig. 4. The selected representative patterns for product nanopowders are presented in Fig. 5 and the calculated structural parameters, relative amounts of phases, and average particle sizes for all samples are included in Table S1 of ESI.‡

The pattern for the manually ground arsenide supports relatively large crystallites (very narrow peaks) displaying some texturing as evidenced by peak (022) with an increased intensity relative to the standard bar chart for cubic GaAs (*cf.* Fig. 5). The ball milled arsenide shows a "no-texture" pattern but the peak bases are significantly broadened pointing out to some degree of material amorphization with a share of crystallites in the nanosized regime. This agrees well with the particle distribution analysis for this material. Interestingly, no other phases are detected which means that the amount of elemental As, of which presence is suggested from Raman measurements (*vide infra*), must be below the method's detection limits. The bulk GaAs wafer shows only two peaks, (002) and (004), consistent with the [100] orientation of the wafer.

The nitride nanopowders from the manually ground precursor and from three temperatures, *i.e.*, 700, 800, and 900 °C, consist of both GaN polytypes and the minor unreacted GaAs; the relative sharpness of diffraction peaks for the latter points out to large particles of the unreacted arsenide. Some unreacted GaAs is found also in the short ball milled sample from the 700 °C-ammonolysis with all remaining products

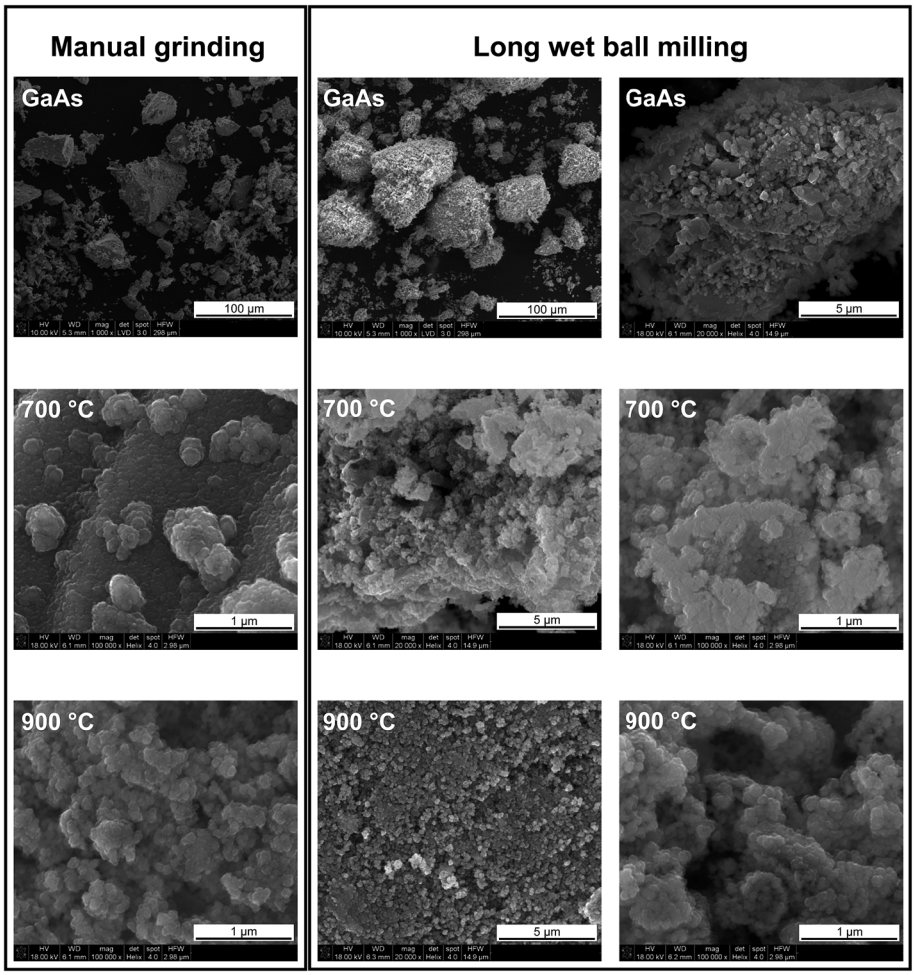

Fig. 2 SEM images of GaAs powdered substrates (top row) and resulting GaN nanopowders from 700 and 900 °C nitridation (middle and bottom row, respectively). The images for solids from manual grinding and long wet ball milling are enclosed in two separate rectangles.

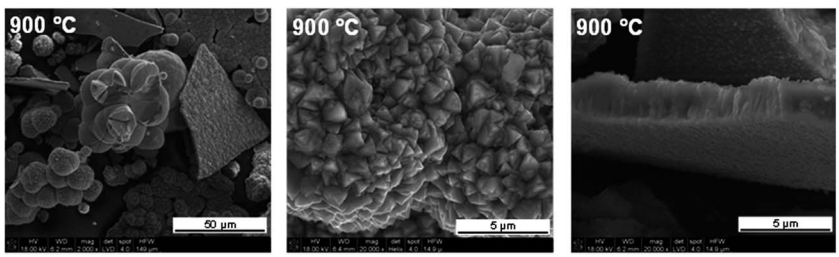

Fig. 3 SEM images of GaN products from nitridation of bulk GaAs wafer, 900 °C, 6 h. Left – fragments of surface layer and interior spheres, middle – details of interior sphere, right – details of surface layer.

showing complete nitridation. The diffraction patterns for the manually ground GaAs and 700 and 800 °C-synthesized nanopowders can be satisfactorily fitted assuming a bimodal size distribution of h-GaN with significantly different average crystallite sizes. This approximation results in two h-GaN fractions (Table S1‡). Interestingly, the ball milled 650 and 700 °C-derived nanopowders are composed exclusively of h-GaN whereas similar nanopowders from the higher temperatures consist of both polytypes. The sole h-GaN polytype is also found in the product after nitridation of the bulk GaAs wafer at 950 °C, 6 h. When comparing this outcome with a related conversion of the wafer at 900 °C, 6 h (76% of h-GaN and 24% of c-GaN), the slightly higher temperature had clearly a detrimental impact on the formation of the metastable c-GaN. The materials made from manually ground GaAs contain relatively more c-GaN than those from ball milled GaAs. The highest content of c-GaN, 65%, is found after the conversion of manually ground GaAs at 900 °C, 6 h; an additional 2 h reaction at this temperature

Table 1 Total specific surface area BET, S_{BET}, mesopore specific surface area, S_{BJH}, and average mesopore size, $D(\text{pore})_{BJH}$ for GaAs substrates and GaN nanopowder products. MG – manual grinding, SBM – short ball milling, LBM – long ball milling

Powder (temperature_time/grinding)	S_{BET} [$m^2\ g^{-1}$]	S_{BJH} [$m^2\ g^{-1}$]	$D(\text{pore})_{BJH}$ [nm]
Substrate GaAs/MG	2	2	6
Substrate GaAs/SBM	5	6	5
Substrate GaAs/LBM	9	21	7
700 °C_90 h/MG	5	6	7
700 °C_90 h/SBM	16	19	13
700 °C_90 h/LBM	26	31	14
800 °C_90 h/MG	3	4	9
800 °C_90 h/SBM	15	17	13
800 °C_90 h/LBM	25	29	10
900 °C_6 h/MG	5	6	7
900 °C_6 h/SBM	15	18	12
900 °C_6 h/LBM	24	28	14

results in no residual GaAs. It is worth to recall that the 900 °C-nitridation of a bulk wafer yields a product with a distinct surface layer and the averaged XRD data indicate 76% of h-GaN and 24% of c-GaN. Although not obvious from Table S1,‡ a detailed pattern analysis in this case supports a pronounced texturing and preferential crystal growth, especially, of the h-GaN component. This could be explained by referring to the morphologies of the surface layer and of the interior as shown in Fig. 3. The h-GaN on the wafer's surface could form a tight layer that would significantly slow down an in-and-out diffusion of reactive species. This would lead to an enhanced GaAs decomposition beneath and nitridation of resulting Ga droplets towards h-GaN seen later in the spherical features of interior (trigonal and hexagonal crystallites in Fig. 3, middle). In conclusion of the XRD study, the ball milled GaAs provides with the exclusive h-GaN at nitridation temperatures of 650–700 °C, as does the conversion of the bulk GaAs wafer at 950 °C, whereas manually ground GaAs and/or other conversion temperatures favor mixtures of both GaN polytypes. Under a broad range of conditions, the ball milling is clearly beneficial for achieving efficient nitridation compared with the manual grinding. Also, XPS spectroscopy for the completely nitride samples shows no content of the plausible residual As by-product.

Raman spectroscopy provides a specific insight into structural properties of the nanopowders by being sensitive to chemical composition (purity), crystalline polytypes, and lattice defects/vacancies.[20] The Raman spectra for selected samples are shown in Fig. 6 and the major peaks from spectra deconvolution can be found in Table S2 of ESI.‡

The spectrum for manually ground GaAs shows the expected two bands for the crystalline arsenide at 264 cm^{-1} (TO) and 285 cm^{-1} (LO).[20c] The very weak and broad features at *ca.* 156 and 239 cm^{-1} are in the region where the LA and TO bands, respectively, were quoted for amorphous GaAs.[20a,20c] The spectrum is thus consistent with a relatively unchanged solid upon grinding. In contrast to this is the spectrum for the ball milled GaAs. The two fundamental bands are also seen although shifted slightly to lower wavenumbers of 261 and 283 cm^{-1}, respectively. However, a striking feature is the presence of two bands at 195 and 243 cm^{-1}, which are very close to those for crystalline elemental As, 198 and 255 cm^{-1}.[20b] The band at 243 cm^{-1} is also very close to the Raman shift recorded for solid gallium metal at 246 cm^{-1}.[20l] Additionally, the broad bands for amorphous GaAs, *ca.* 160 and 240 cm^{-1}, and amorphous As, 220 cm^{-1}, are reasonably refined in the broad base of the entire group of bands in the 180–300 cm^{-1} range. First, the presence of amorphous GaAs supports pronounced size changes to the arsenide upon high energy ball milling. Second, the ball milling seems to cause, additionally, some decomposition of the compound to elements. The presence of elemental Ga can be especially important in the subsequent nitridation of the ball milled GaAs, as described later.

All nitride products show bands above 300 cm^{-1} and, especially, in the 500–750 cm^{-1} range expected for GaN. Additionally, the 700 and 900 °C-derived nanopowders from the manual grinding series show the bands for unreacted GaAs (Fig. 6, dotted lines) that are also detected by XRD at a few percent level (Table S1‡). The 700 and 800 °C-derived nanopowders from the ball milling series appear to contain the residual bands for elemental As, the latter originally present in the precursor (Fig. 6, solid lines). This would suggest some remnant quantities of As being retained in the products and imply longer hold times to sublime it out.

In principle, there are two modes expected for c-GaN, 552–555 cm^{-1} (TO) and 739 cm^{-1} (LO) and six modes for h-GaN, 144 cm^{-1} (E_2 low), 532 cm^{-1} (A_1-TO), 554–559 cm^{-1} (E_1-TO), 568–569 cm^{-1} (E_2 high), 734–735 cm^{-1} (A_1-LO), and 741 cm^{-1} (E_1-LO).[20g,h] All these eight bands are grouped in two shift ranges, *i.e.*, 530–570 cm^{-1} and 730–740 cm^{-1}, and when taking into account the proximity of many of them, the bands merging/superposition is a matter of fact. That is the reason that,

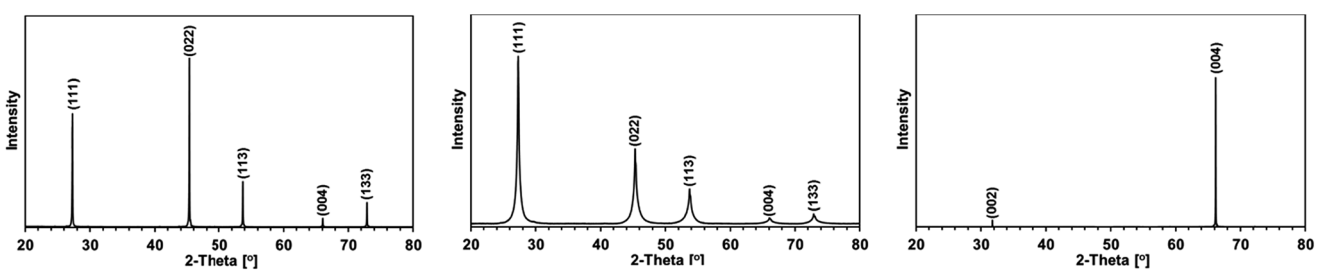

Fig. 4 XRD patterns for GaAs substrates: left – manually ground, middle – long ball milled, right – [100] oriented bulk wafer.

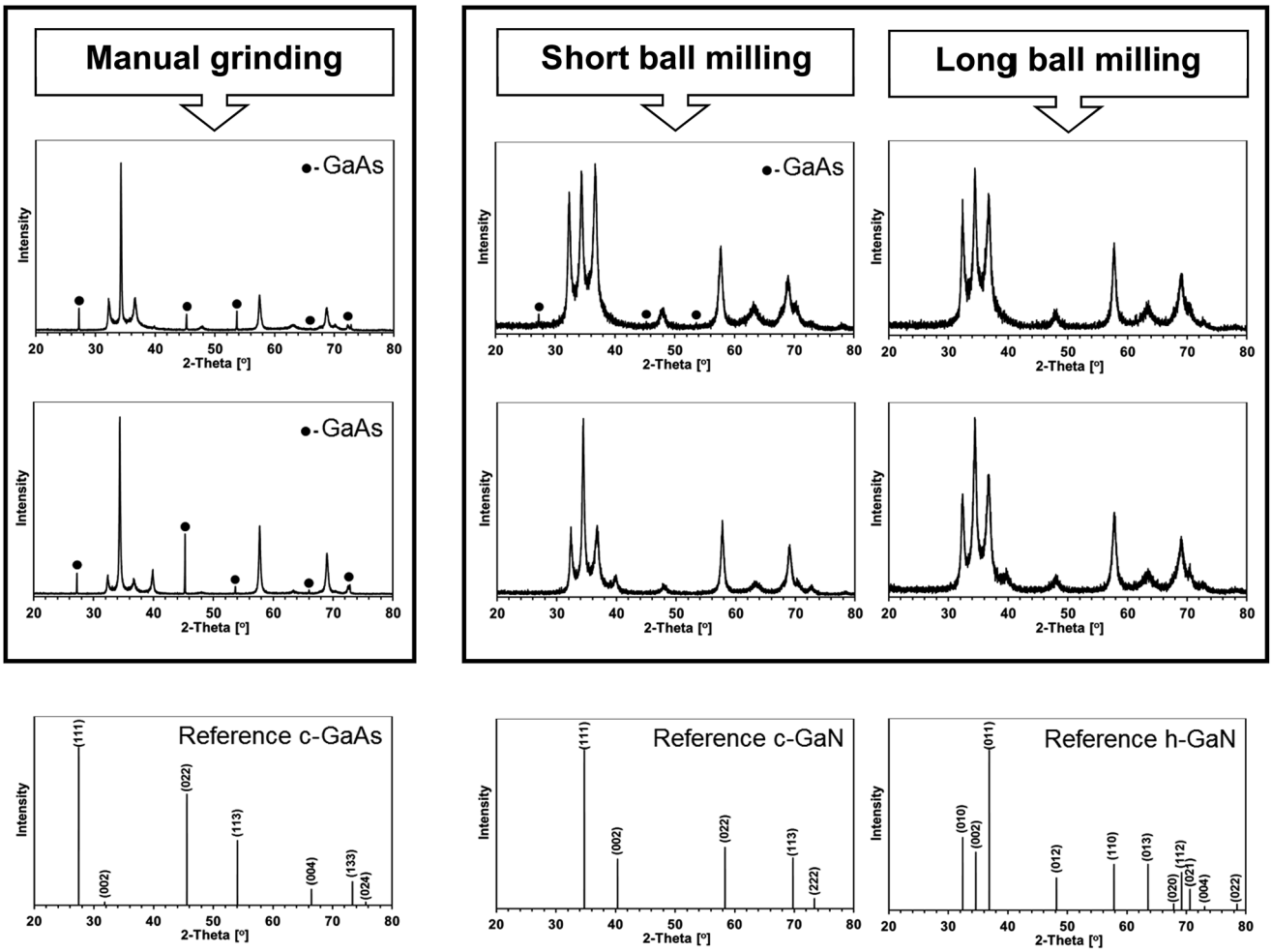

Fig. 5 XRD patterns for nitride products after ammonolysis at selected temperatures: top row – 700 °C, 90 h; middle row – 900 °C, 6 h; bottom row – reference bar charts for: left – cubic GaAs (ICSD 98-004-1981), middle – cubic GaN (ICSD 98-015-6260), right – hexagonal GaN (ICSD 98-002-5676). Rectangle on the left includes patterns for products from manually ground GaAs. Rectangle on the right includes patterns for products from short and long ball milled GaAs.

actually, two broad and frequently asymmetrical features are seen there for all the products. The actual peak positions in Table S2‡ are derived from best fitting deconvolution of the features that introduces also some uncertainties about how accurate are the positions. However, many qualitative observations can be made regarding the presence of both GaN polytypes. For instance, when considering the nanopowders from the manual grinding series, the relative intensity of the composite band in the 530–570 cm^{-1} range relative to the band in the 730–740 cm^{-1} range grows with conversion temperature. This, at the same time, is associated with increased proportions of c-GaN in the products. Other things being equal, one can assume that this behavior is due to the proportionally increased intensity of the TO band in c-GaN. The bands fitted between 600 and 700 cm^{-1}, which form the valley between the ranges, have been assigned either to the B_1 (low) silent mode in h-GaN upon activation in low symmetry defected structures[20i] or to N-vacancies in h-GaN.[20j] Also, a noticeable red shift of the expected 730–740 cm^{-1} composite band to the 700 cm^{-1} range is likely a consequence of defected structures of the GaN nanopowders as observed earlier by us for the related GaP/NH_3 and $GaSb/NH_3$ nitridation systems.[10,11] There are also other bands which can be assigned to GaN nanostructures. They include the bands in the 150, 300, and 400–420 cm^{-1} ranges with the first one due to the E_2 (low) mode in h-GaN[20g] and the latter two invoking N-vacancies[20j] or B_1 (low) activated silent mode in h-GaN[20i] while both confirming defected structures. The broad and sometimes strong band in the 200 cm^{-1} range is in the region expected for various forms of As and if so it would suggest some residual amorphous arsenic since no crystalline As is detected by XRD.

Solid state ^{71}Ga MAS NMR spectroscopy provides a further insight into structural properties of the products. The spectra of the GaN nanopowders and of the reference GaAs are shown in Fig. 7 and the peak positions from curve deconvolutions are summarized in Table 2.

The spectra of all products prepared from manually ground GaAs contain as a minor feature a sharp peak at 216 ppm consistent with some unreacted GaAs, which is also substantiated by XRD. The peak for the long ball milled sample is broader

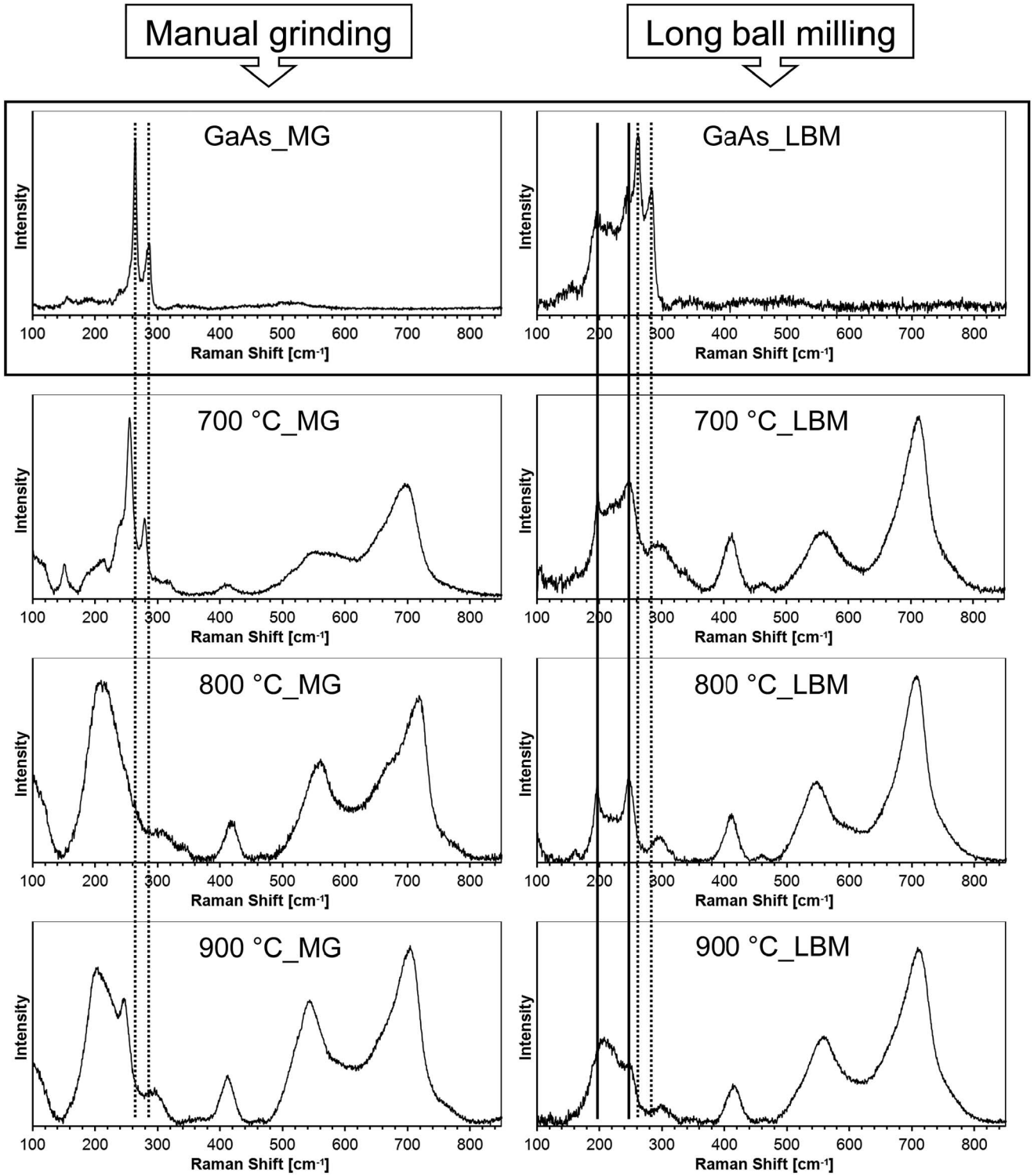

Fig. 6 Micro-Raman spectra for GaAs substrates and nitrided products from selected conversion temperatures of 700, 800, and 900 °C. MG – manual grinding, LBM – long ball milling. Reference spectra for GaAs are shown in rectangle, top row. Dotted and solid vertical lines indicate positions of the Raman shifts in crystalline GaAs and As, respectively.[20a–c]

compared with the manually ground option which supports higher degree of amorphization in the former. Based on our earlier NMR studies, each of the GaN polytypes may have optionally two distinct gallium resonances, *i.e.*, for h-GaN at *ca.* 325–330 ppm and 415–440 ppm and for c-GaN a similar pair of resonances which is moved by some 30–40 ppm downfield to 350–360 and 420–480 ppm, respectively.[5i,10,11] The higher field peak in a pair, *i.e.*, at lower ppm's, is relatively sharp

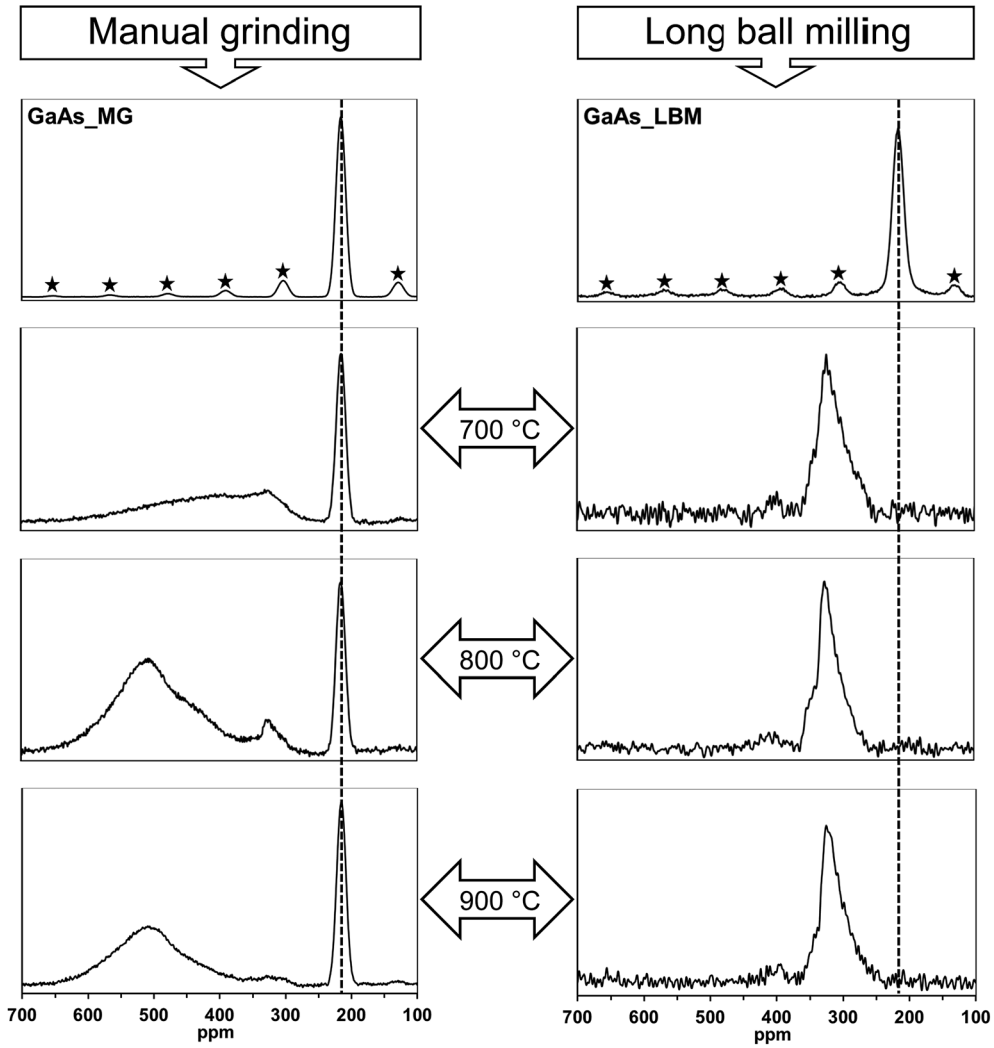

Fig. 7 Solid state ^{71}Ga MAS NMR spectra of GaAs (reference) and GaN nanopowders from nitridation of GaAs. MG – manual grinding, LBM – long mall milling. Asterisks indicate spinning side bands; dotted lines indicate positions of gallium resonance in GaAs.

corresponding to a good uniformity of the short range structure order in well crystallized GaN whereas the respective lower field peak is significantly broadened. From somewhat controversial literature data, the lower field peak has been assigned either to a postulated N-deficient phase of the type GaN_{1-x} $(0 < x < 1)$[12b,21] or, alternatively, to a Knight shift due to the presence of conduction electrons in the semiconductor.[22] In our earlier studies, we observed for the h-GaN polytype an increasing intensity of the lower field broad peak at the expense of the higher field peak upon nitride annealing under ammonia at higher temperatures than the conversion temperature. Therefore, it appears that the temperature/time-induced nanopowder recrystallization during such annealing, although results by XRD criteria in better crystallinity may, at the same time, introduce specific short range crystal defects such as N-vacancies and/or impurity oxygen incorporation into regrown lattices.

Table 2 ^{71}Ga MAS NMR peak positions for GaN nanopowders. MG – manual grinding, LBM – long ball milling

		Chemical shift [ppm]					
		700 °C, 90 h		800 °C, 90 h		900 °C, 6 h	
GaN polytype	Resonance position	MG	LBM	MG	LBM	MG	LBM
h-GaN	Higher field	326	325	327	326	324	326
	Lower field	410	410	440	410	425	410
c-GaN	Higher field	355	—	350	350	355	350
	Lower field	500	—	510	—	510	—

A striking difference between the two studied groups of nanopowders is the distinct resonance pattern in each group. For the materials made from ball milled GaAs, the dominant if not exclusive are the higher field peaks for both GaN polytypes, 325–326 (h-GaN) and 350 ppm (c-GaN), with the relative intensities reflecting the polytype proportions estimated earlier from the XRD data. The respective lower field peaks, *i.e.*, the barely seen peaks at 410 for h-GaN with none seen for c-GaN are on the

verge of detection, if any at all, since they are in the region of the spinning side band. All this constitutes a strong argument for the stoichiometric, well crystallized gallium nitride in both polytype forms in these nanopowders. This peak's pattern can be contrasted with the spectra for the other group of nanopowders. The manual grinding resulted in the formation of materials which showed the lower field peaks at 500–510 ppm as the predominant feature at least for the 800 and 900 °C-conversions. Based on our experience, these peaks could be assigned to the defected/nonstoichiometric c-GaN. One has to notice, though, their shift to lower fields from the often commonly observed 470–480 ppm range now to the values close and exceeding 500 ppm. The high intensity of these peaks is consistent with the c-GaN being severely defected which could be understood in terms of various disorder impinged onto the strained, gradually collapsing substrate's cubic lattice by N-for-As element replacement reactions. The observed shift to the 500 ppm range could also imply some arsenic atoms still present in the cubic lattice as substitutional impurity.

The UV-vis spectra shown in Fig. 8 (measured optical spectra and derived Kubelka–Munk transformations) provided yet another angle to probe the structural/electronic integrity of the nanopowders. The calculated specific electronic transitions are collected in Table 3. For gallium nitride materials, E_g1 at 2.2–2.9 eV corresponds to band tail transitions linked to various impurities, disorder, and defects and E_g2 at 2.9–3.6 eV is related to the material's energy bandgap.[23] It is apparent that all nanopowders show in addition to the structure/crystallite size related E_g2 transitions also the defect/disorder related E_g1 transitions. In this regard, various defect features are evident

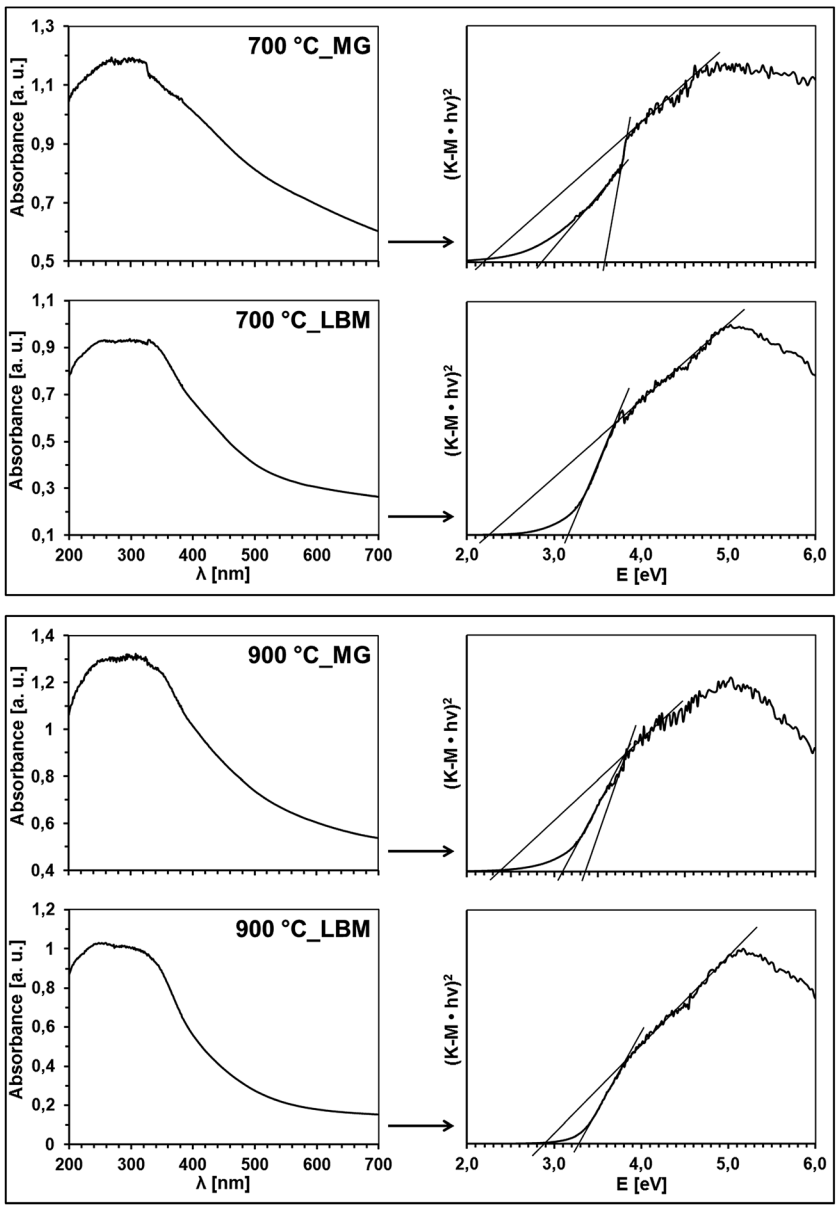

Fig. 8 UV-vis optical spectra (left panel) and derived Kubelka–Munk transformations (right panel) for GaN nanopowders from 700 °C, 90 h and 900 °C, 6 h conversions. MG – manual grinding, LBM – long ball milling.

Table 3 UV-vis derived E_g values for GaN nanopowders. MG – manual grinding, LBM – long ball milling

Nitridation	Grinding	E_g1 [eV]	E_g2(I) [eV]
700 °C, 90 h	MG	2.5	2.9/3.6
	LBM	2.3	3.2
800 °C, 90 h	MG	2.2	3.1/3.4
	LBM	2.2	3.2
900 °C, 90 h	MG	2.4	3.1/3.4
	LBM	2.9	3.3

also in the Raman and NMR studies of the nanopowders as discussed earlier.

It is instructive to recall that for bulk h-GaN the bandgap transitions are expected at E_g2 equal to *ca.* 3.4 eV whereas a shift to higher energies (blue shift) is expected for nanocrystallites with sizes below the Bohr radius quoted in the range 3–11 nm.[24] The E_g2 value at 3.6 eV for the GaN nanopowder from 700 °C, 90 h/MG (Table 3, top line) could be a manifestation of such a shift since by XRD the material contains a h-GaN fraction with sizes much below 11 nm (Table S1‡). This powder is characteristic also of a second and major E_g2 transition with a rather unusually low value of 2.9 eV. In the absence of other bandgap-related transitions in this bi-polytypic material, we tentatively assign the transition to the arsenic-doped c-GaN polytype. It comes down to a red shift from the 3.2 eV value for c-GaN, *i.e.*, in the expected direction upon As-for-N substitution. It is also consistent with the somewhat increased lattice constant for c-GaN from the theoretical a = 4.50–4.51 Å to the measured 4.52 Å (Table S1‡) that implies bigger for smaller atom substitutions. As discussed earlier, topochemical replacement of As by N in c-GaAs would mean collapsing of the initial cubic lattice of a = 5.65 Å to the cubic GaN of a = 4.50–4.51 Å. It is to recall also that $GaN_{1-x}As_x$ alloys with up to a few percent As were reported.[18]

Pathways in ammonolysis of c-GaAs

The overall picture that emerges from studying the ammonolysis of various ground materials forms of GaAs is consistent with a specific reactivity pattern in the system as illustrated in Fig. 9. It includes two distinct pathways entangled in a fine interplay that is, mainly, way of grinding/milling and temperature dependent. One pathway leads to the thermodynamically favored h-GaN *via* ammonolysis of molten Ga droplets from decomposition of GaAs, the latter taking place in part during high energy ball milling and/or at increased temperatures (Fig. 9, pathways to the right). The presence of molten Ga initiates and supports at lower temperatures of 650–700 °C the nitridation conversion to h-GaN whereas at 800–900 °C c-GaN is concurrently formed. Similarly, the precursor decomposition prevails in the 950 °C-conversion of GaAs bulk wafer yielding exclusively h-GaN. The other pathway that additionally leads to the topochemically stimulated formation of c-GaN is specific for rather coarse GaAs particles (such as those abundant in the manually ground substrate) and at temperatures in the 700–900 °C range (Fig. 9, pathways to the left). But there could not be found a wide enough range of conditions to afford an exclusive formation of c-GaN, with the highest proportion of the latter of 65% made at 900 °C, 6 h, from the manually ground GaAs.

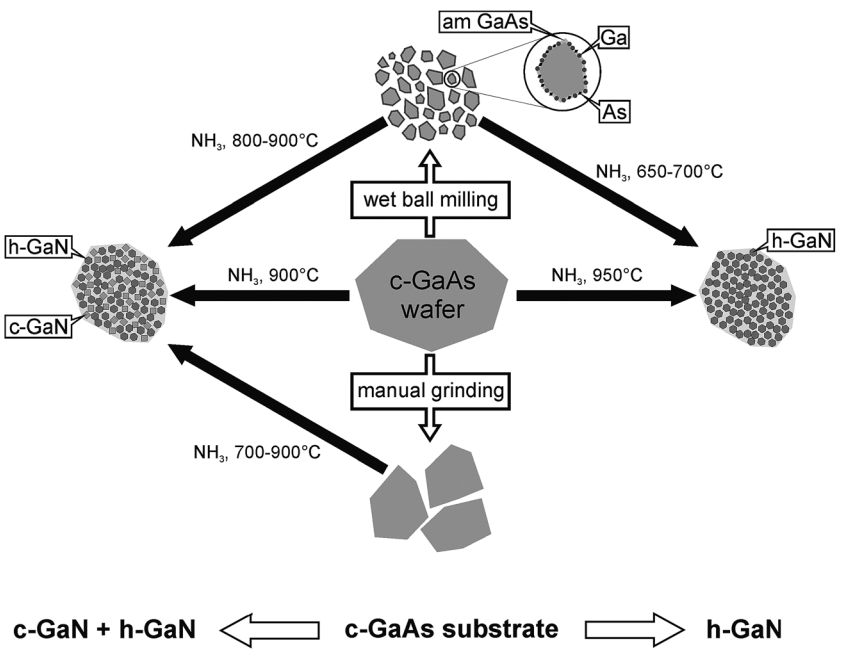

Fig. 9 Ammonolytical conversion of mono and polycrystalline c-GaAs to nanocrystalline powders of h-GaN and c-GaN. am GaAs – amorphous GaAs. To the right – thermodynamically favored formation of h-GaN *via* decomposition of c-GaAs, to the left – in addition to thermodynamics, topochemically controlled formation of c-GaN *via* N-for-As metathesis in c-GaAs.

Conclusions

The single-step ammonolysis of monocrystalline, polycrystalline or amorphized gallium arsenide c-GaAs in the 650–950 °C temperature range is a convenient way of making oxygen-free GaN nanopowders either as a sole hexagonal polytype h-GaN or as a mixture of the hexagonal and cubic polytypes, h-GaN and c-GaN. The formation of the polytypes is a consequence of two competing mechanisms of nitridation linked to the different in origin factors, namely, thermodynamics and topochemistry. In this regard, the thermodynamically favored synthesis of stable h-GaN appears to proceed *via* c-GaAs decomposition and elemental Ga formation. The high energy ball milling that introduces substrate amorphization and partial decomposition as well as moderate conversion temperatures support this pathway by way of GaAs thermal instability. Also, the reactivity of the monocrystalline GaAs wafer at extreme temperatures is dominated by the same mechanism. On the other hand, the topochemically controlled synthesis of metastable c-GaN in part operates for coarse particles of c-GaAs at a suitable temperature range when N-for-As replacement reactions appear to take place fast enough to successfully compete with decomposition. In order to remove the As by-product by sublimation sufficiently long hold times are necessary. A multipronged characterization of the resulting GaN nanopowders including such analytical methods as powder XRD, Raman, UV-vis, and ^{69,71}Ga NMR spectroscopies is necessary to pinpoint their diverse structure/disorder/purity/electronic properties. A challenging question of the plausible structural relationship between the h-GaN and c-GaN domains within the nitride particles in the low nanosized range requires well focused future HRTEM studies coupled with unconventional XRD measurements and data analysis. The nitridation of GaAs, together with the previously published studies on the related systems of GaP/NH_3 and GaSb/NH_3, makes now plausible to have control over a wide range of GaN polytype mixture compositions including a pure h-GaN variety, average particle sizes, morphologies, and structural integrity. However, preparations of exclusively c-GaN nanopowders still remain an open question.

Acknowledgements

The study was supported by the Polish National Science Center (NCN), Grant No. 2013/09/B/ST5/01223.

References

1 (*a*) I. Akasaki, *Angew. Chem., Int. Ed.*, 2015, **54**, 7750–7763; (*b*) H. Amano, *Angew. Chem., Int. Ed.*, 2015, **54**, 7764–7769; (*c*) S. Nakamura, *Angew. Chem., Int. Ed.*, 2015, **54**, 7770–7788; (*d*) H. P. Maruska and W. C. Rhines, *Solid-State Electron.*, 2015, **111**, 32–41; (*e*) S. S. Khludkov, I. A. Prudaev and O. P. Tolbanov, *Russ. Phys. J.*, 2013, **55**, 903–909; (*f*) M. S. Kang, C. H. Lee, J. B. Park, H. Yoo and G. C. Yi, *Nano Energy*, 2012, **1**, 391–400.

2 (*a*) T. Hashimoto, E. Letts and S. Hoff, *Sens. Mater.*, 2013, **25**, 155–164; (*b*) R. Dwilinski, R. Doradzinski, J. Garczynski, L. Sierzputowski, R. Kucharski, M. Zajac, M. Rudzinski, R. Kudrawiec, W. Strupinski and J. Misiewicz, *Phys. Status Solidi A*, 2011, **208**, 1489–1493; (*c*) M. Bockowski, P. Strak, I. Grzegory and S. Porowski, *Technology of gallium nitride crystal growth*, Book Series: Springer Series in Materials Science, 2010, vol. 133, pp. 207–234; (*d*) V. Avrutin, D. Silversmith, Y. Mori, F. Kawamura, Y. Kitaoka and H. Morkoc, *Proc. IEEE*, 2010, **98**, 1302–1315.

3 (*a*) M. A. Malik, M. Afzaal and P. O'Brien, *Chem. Rev.*, 2010, **110**, 4417–4446; (*b*) B. Mazumder and A. L. Hector, *J. Mater. Chem.*, 2009, **19**, 4673–4686; (*c*) C. N. R. Rao, C. R. C. Vivekchand, K. Biswas and A. Govindaraj, *Dalton Trans.*, 2007, 3728–3749.

4 (*a*) S. Stelmakh, A. Swiderska-Sroda, G. Kalisz, S. Gierlotka, E. Grzanka, B. Palosz, M. Drygas, J. F. Janik and R. T. Paine, *Proceedings of the International Conference on Nanoscience and Technology, Basel, Switzerland, July 30th–Aug 4th, 2006*, Institute of Physics Publishing, Philadelphia, PA, 2006; (*b*) E. Grzanka, S. Stelmakh, S. Gierlotka, A. Swiderska-Sroda, G. Kalisz, B. Palosz, M. Drygas, J. F. Janik and R. T. Paine, European Powder Diffraction Conference, EPDIC-10, Geneva, Switzerland, Sept. 1-4, 2006 – Z. Kristallogr., 2007, 26, MS11; (*c*) J. Borysiuk, P. Caban, W. Strupinski, S. Gierlotka, S. Stelmakh and J. F. Janik, *Cryst. Res. Technol.*, 2007, **42**, 1291–1296; (*d*) Polish patent No. P-378458: Way to make sintered gallium nitride GaN; patent issued as published in *Wiadomości Urzędu Patentowego* (News of the Polish Patent Office), No. 2/2012, Feb. 29, 2012; (*e*) M. Drygas, J. F. Janik, J. Gosk, S. Gierlotka, B. Palosz and A. Twardowski, *J. Eur. Ceram. Soc.*, 2016, **36**, 1033–1044.

5 (*a*) R. L. Wells and J. F. Janik, *Eur. J. Solid State Inorg. Chem.*, 1996, **33**, 1079–1090; (*b*) J. F. Janik and R. L. Wells, *Chem. Mater.*, 1996, **8**, 2708–2711; (*c*) J. F. Janik and R. L. Wells, *Inorg. Chem.*, 1997, **36**, 4135–4137; (*d*) J. L. Coffer, M. A. Johnson, L. Zhang, R. L. Wells and J. F. Janik, *Chem. Mater.*, 1997, **9**, 2671–2673; (*e*) J. F. Janik, R. L. Wells, J. L. Coffer, J. V. St. John, W. T. Pennington and G. L. Shimek, *Chem. Mater.*, 1998, **10**, 1613–1622; (*f*) J. L. Coffer, T. W. Zerda, R. Appel, R. L. Wells and J. F. Janik, *Chem. Mater.*, 1999, **11**, 20–22; (*g*) R. L. Jouet, A. P. Purdy, R. L. Wells and J. F. Janik, *J. Cluster Sci.*, 2002, **13**, 469–486; (*h*) J. F. Janik, M. Drygas, S. Stelmakh, E. Grzanka, B. Palosz and R. T. Paine, *Phys. Status Solidi A*, 2006, **203**, 1301–1306; (*i*) M. Drygas, Z. Olejniczak, E. Grzanka, M. M. Bucko, R. T. Paine and J. F. Janik, *Chem. Mater.*, 2008, **20**, 6816–6828; (*j*) M. Drygas and J. F. Janik, *Mater. Chem. Phys.*, 2012, **133**, 932–940.

6 (*a*) C. Y. Yeh, Z. W. Lu, S. Froyen and A. Zunger, *Phys. Rev. B: Condens. Matter Mater. Phys.*, 1992, **46**, 10086; (*b*) A. Zoroddu, F. Bernardini, P. Ruggerone and V. Fiorentini, *Phys. Rev. B: Condens. Matter Mater. Phys.*, 2001, **64**, 045208.

7 S. V. Novikov, N. M. Stanton, R. P. Campion, C. T. Foxon and A. J. Kent, *J. Cryst. Growth*, 2008, **310**, 3964–3967.

8 (*a*) A. P. Purdy, R. J. Jouet and C. F. George, *Cryst. Growth Des.*, 2002, **2**, 141–145; (*b*) W. Y. Wang, Y. P. Xu, D. F. Zhang and X. L. Chen, *Mater. Res. Bull.*, 2001, **36**, 2155–2162.

9 (*a*) B. W. Jacobs, V. M. Ayres, M. P. Petkov, J. B. Halpern, M. He, A. D. Baczewski, K. McElroy, M. A. Crimp, J. M. Zhang and H. C. Shaw, *Nano Lett.*, 2007, **7**, 1435–1438; (*b*) S. Suandon, S. Sanorpim, K. Yoodee and K. Onabe, *Thin Solid Films*, 2007, **515**, 4393–4396; (*c*) B. W. Jacobs, V. M. Ayres, M. A. Crimp and K. McElroy, *Nanotechnology*, 2008, **19**, 405706; (*d*) J. A. Jegier, S. McKernan, A. P. Purdy and W. L. Gladfelter, *Chem. Mater.*, 2000, **12**, 1003–1010; (*e*) S. V. Cherepanova, *J. Struct. Chem.*, 2012, **53**, S109–S132.

10 M. Drygas, M. Sitarz and J. F. Janik, *RSC Adv.*, 2015, **5**, 106128–106140.

11 M. Drygas, P. Jelen, M. M. Bucko, Z. Olejniczak and J. F. Janik, *RSC Adv.*, 2015, **5**, 82576–82586.

12 (*a*) A. Addamiano, *J. Electrochem. Soc.*, 1961, **108**, 1072; (*b*) W. S. Jung, O. H. Han and S. A. Chae, *Mater. Chem. Phys.*, 2006, **100**, 199–202.

13 M. Drygas, M. M. Bucko, E. Grzanka and J. F. Janik, *Curr. Nanosci.*, 2013, **9**, 173–182.

14 A. S. Jordan and A. Robertson, *J. Mater. Sci.: Mater. Electron.*, 1993, **4**, 215–224.

15 (*a*) Ch. Heyn and D. E. Jesson, *Appl. Phys. Lett.*, 2015, **107**, 161601; (*b*) J. Tersoff, D. E. Jesson and W. X. Tang, *Phys. Rev. Lett.*, 2010, **105**, 035702.

16 (*a*) J. Wu, Z. M. Wang, A. Z. Li, M. Benamara, S. B. Li and G. J. Salamo, *Plos One*, 2011, **6**, e20765; (*b*) C. Somaschini, S. Bietti, N. Koguchi and S. Sanguinetti, *Nano Lett.*, 2009, **9**, 3419–3424; (*c*) M. Yamagiwa, T. Mano, T. Kuroda, T. Tateno, K. Sakoda, G. Kido, N. Koguchi and F. Minami, *Appl. Phys. Lett.*, 2006, **89**, 113115.

17 K. Laaksonen, H.-P. Komsa, E. Arola, T. T. Rantala and R. M. Nieminen, *J. Phys.: Condens. Matter*, 2006, **18**, 10097–10114.

18 (*a*) A. Kimura, H. F. Tang and T. F. Kuech, *J. Cryst. Growth*, 2004, **265**, 71–77; (*b*) J. Wu, W. Walukiewicz, K. M. Yu, J. D. Denlinger, W. Shan, J. W. III Ager, A. Kimura, H. F. Tang and T. F. Kuech, *Phys. Rev. B: Condens. Matter Mater. Phys.*, 2004, **70**, 115214.

19 N. Urakami, K. Yamane, H. Sekiguchi, H. Okada and A. Wakahara, *J. Cryst. Growth*, 2016, **435**, 19–23.

20 (*a*) J. Bandet, K. Aguir, D. Lollman, A. Fennouh and H. Carchano, *Jpn. J. Appl. Phys.*, 1997, **36**, 11–18; (*b*) G. P. Schwartz, B. V. Dutt and G. J. Gualtieri, *Appl. Phys. Lett.*, 1981, **39**, 52–54; (*c*) T. Salminen, J. Dahl, M. Tuominen, P. Laukkanen, E. Arola and T. Niemi, *Opt. Mater. Express*, 2012, **2**, 799–813; (*d*) G. Y. Yu, Z. X. Shen, L. Liu and W. X. Sun, *Mater. Sci. Semicond. Process.*, 2001, **4**, 581–584; (*e*) T. Prokofyeva, T. Sauncy, M. Seon, M. Holtz, Y. Qiu, S. Nikishin and H. Temkin, *Appl. Phys. Lett.*, 1998, **73**, 1409–1411; (*f*) P. Panpech, S. Vijarnwannaluk, S. Sanorpim, W. Ono, F. Nakajima, R. Katayama and K. Onabe, *J. Cryst. Growth*, 2007, **298**, 107–110; (*g*) H. Harima, *J. Phys.: Condens. Matter*, 2002, **14**, R967–R993; (*h*) M. Giehler, M. Ramsteiner, O. Brandt, H. Yang and K. H. Ploog, *Appl. Phys. Lett.*, 1995, **67**, 733–735; (*i*) F. J. Manjon, B. Mari, J. Serrano and A. H. Romero, *J. Appl. Phys.*, 2005, **97**, 053516; (*j*) M. Katsikini, K. Papagelis, E. C. Paloura and S. Ves, *J. Appl. Phys.*, 2003, **94**, 4389–4394; (*k*) J. Q. Ning, S. J. Xu, D. P. Yu, Y. Y. Shan and S. T. Lee, *Appl. Phys. Lett.*, 2007, **91**, 103117; (*l*) J. A. Creighton and R. Withnall, *Chem. Phys. Lett.*, 2000, **326**, 311–313.

21 (*a*) W. S. Jung, C. Park and S. Han, *Bull. Korean Chem. Soc.*, 2003, **24**(7), 1011–1013; (*b*) W. S. Jung, *Mater. Lett.*, 2006, **60**, 2954–2957; (*c*) B. Schwenzer, J. Hu, R. Seshadri, S. Keller, S. P. DenBaars and U. K. Mishra, *Chem. Mater.*, 2004, **16**, 5088–5095; (*d*) B. Schwenzer, J. Hu, Y. Wu and U. K. Mishra, *Solid State Sci.*, 2006, **8**, 1193–1201.

22 (*a*) J. P. Yesinowski and A. P. Purdy, *J. Am. Chem. Soc.*, 2004, **126**, 9166–9167; (*b*) J. P. Yesinowski, *Phys. Status Solidi C*, 2005, **2**(7), 2399–2402; (*c*) J. P. Yesinowski, A. P. Purdy, H. Wu, M. G. Spencer, J. Hunting and F. J. DiSalvo, *J. Am. Chem. Soc.*, 2006, **128**, 4952–4953; (*d*) J. P. Yesinowski, in *Solid State NMR Book Series: Topics in Current Chemistry*, ed. J. C. C. Chan, Springer, 2012, vol. 306, ch. Solid-state NMR of inorganic semiconductors, pp. 229–312.

23 I. Akyuz, S. Kose, F. Atay and V. Bilgin, *Semicond. Sci. Technol.*, 2006, **21**, 1620–1626.

24 (*a*) P. Ramvall, S. Tanaka, S. Nomura, P. Riblet and Y. Aoyagi, *Appl. Phys. Lett.*, 1998, **73**, 1104–1106; (*b*) X. L. Chen, J. N. Li, Y. G. Cao, Y. C. Lan, H. Li, M. He, C. Y. Wang, Z. Zhang and Z. Y. Qiao, *Adv. Mater.*, 2000, **12**, 1432–1434.